MOLECULAR PHYSICS, 1985, VOL. 55, NO. 5, 1171–1192

The hard ellipsoid-of-revolution fluid
I. Monte Carlo simulations

by D. FRENKEL
Fysisch Laboratorium, Rijksuniversiteit, Utrecht, The Netherlands
and B. M. MULDER
Institute for Theoretical Physics, Rijksuniversiteit, Utrecht, The Netherlands

(*Received 8 March 1985 ; accepted 25 March 1985*)

We present the results of Monte Carlo simulations on a system of hard ellipsoids of revolution with length-to-breadth ratios $a/b = 3$, 2·75, 2, 1·25 and $b/a = 3$, 2·75, 2, 1·25. We identify four distinct phases, viz. isotropic fluid, nematic fluid, ordered solid and plastic solid. The coexistence points of all first order phase transitions are located by performing absolute free energy computations for all coexisting phases. We find nematic phases only for $a/b \geqslant 2{\cdot}75$ and $a/b \leqslant 1/2{\cdot}75$. A plastic solid is only observed for $1{\cdot}25 \geqslant a/b \geqslant 0{\cdot}8$. It is found that the phase diagram is surprisingly symmetric under interchange of the major and minor axes of the ellipsoids.

1. INTRODUCTION

In this paper we present the results of a series of Monte Carlo simulations on model systems consisting of hard ellipsoids of revolution. Hard ellipsoids of revolution, henceforth referred to as HERs, constitute a very simple model for non-spherical molecules. The surface of a HER is given by the following equation:

$$\frac{z^2}{a^2} + \frac{(x^2 + y^2)}{b^2} = 1, \tag{1.1}$$

where $2a$ is the length of the molecule along its symmetry axis and $2b$ is the length of any axis perpendicular to the symmetry axis. In equation (1) molecule-fixed coordinates have been used for convenience. The shape of a HER is determined by the axial ratio $x \equiv (a/b)$. By varying x from 0 to ∞ the shape of the HER goes from extremely oblate ('platelets': $x \to 0$) through spherical ('hard spheres'; $x = 1$) to extremely prolate ('needles'; $x \to \infty$). A considerable amount is known about the properties of HER's in the limiting cases $x = 0$, ∞ and, in particular, $x = 1$.

For hard spheres ($x = 1$), a wealth of numerical data is available on both equilibrium and transport properties. In particular, the equation of state of both the fluid and the solid branches are known to a high degree of accuracy. The

location of the solid-fluid phase transition has been determined by Hoover and Ree [1]. The case $x = \infty$ ('needles') has been studied numerically in the semi-dilute ($\rho a^2 b \ll 1$)regime [2]. For the case $\rho a^2 b = O(1)$, the equation of state of ellipsoidal needles follows directly from the solution of the Onsager model for long, thin spherocylinders [3] because the excluded volume of a pair of ellipsoidal needles is of the form $V_{\mathrm{EXCL}}(\theta) = 4\pi a^2 b|\sin\theta|$ where θ is the angle between the two needles. This expression for the $V_{\mathrm{EXCL}}(\theta)$ follows directly from the known expression for the pair excluded volume of infinitely thin platelets and the symmetry relation between the excluded volume of particles with inverse length-to-breadth ratios given in [8]. The above expression for $V_{\mathrm{EXCL}}(\theta)$ for needle-like ellipsoids should be compared with the result for sperocylinders of length L and diameter d, in the limit $(L/d) \to \infty$, $V_{\mathrm{EXCL}}(\theta) = L^2 d|\sin\theta|$. In both systems all virial coefficients higher than the second are negligible. Hence by simply substituting $4\pi a^2 b$ for $L^2 d$ in the expression for $V_{\mathrm{EXCL}}(\theta)$, all known results for the Onsager model can be directly applied to hard ellipsoids of revolution in the limit $x \to \infty$. It follows that a fluid of hard ellipsoidal needles undergoes a phase transition from the isotropic to the nematic phase at a reduced number density $\rho_{\mathrm{I}} B_2 = 3{\cdot}30$ (where B_2 is the second virial coefficient) while, at coexistence, $\rho_{\mathrm{N}} B_2 = 4{\cdot}16$ [4]. Note that in the limit $x = \infty$ this transition takes place at zero packing fraction ($\rho_{\mathrm{IN}}(4\pi/3)ab^2 \to 0$, as $x \to \infty$). No data are available on the properties of ellipsoidal needles at finite packing fractions. Hard platelets ($x = 0$) have been studied numerically at densities such that $\rho b^3 = O(1)$ [5].

From these simulations it is known that hard platelets undergo an isotropic–nematic transition at $\rho_{\mathrm{I}} B_2 = 2{\cdot}49$ ($\rho_{\mathrm{N}} B_2 = 2{\cdot}54$). Hence we know that in the limits $x \to 0$ and $x \to \infty$ there is a first order phase transition from the isotropic fluid phase to the nematic phase at a packing fraction $\eta_{\mathrm{IN}} = O(x)$ ($O(1/x)$ for needles). The behaviour of ellipsoidal platelets and needles has, thus far not been studied at finite packing fraction. However, from the work of Hoover and Ree it is known that for $x = 1$ there is a first order phase transition from the (isotropic) fluid phase to the crystalline phase, at a packing fraction $\eta_{\mathrm{F}} \approx 0{\cdot}49$. It seems likely, that freezing of the nematic phases of platelets and needles will take place at a finite packing fraction as well. Of course, the exact location of the melting point of HERs will depend on molecular shape, but this variation is expected to be much less drastic than the change of the isotropic–nematic transition with molecular shape. Typically, the I–N transition will take place at a number density ρ, such that $\rho_{\mathrm{IN}} V_{\mathrm{EXCL}} = O(1)$, while freezing takes place when $\rho_{\mathrm{F}} V_0 \simeq O(1)$ (here V_0 stands for the molecular proper volume). Hence, as the molecules become more spherical ρ_{IN} will approach ρ_{F}, and eventually the isotropic–nematic transition will be preempted by the freezing transition. In other words, there should be a finite range of values of the length-to-breadth ratio x, around $x = 1$, where no stable nematic phase is possible. Although the crystal structures of HERs may be different from the structure of the hard-sphere solid, there is a simple relation at close packing. A uniform compression or expansion by a factor x, along any axis, transforms the close packed hard-sphere solid into a close packed solid of HERs with axial ratio x. This transformation does not change the packing fraction. Hence the density of closest packing of HERs is at least as high as the density of closest packing of hard spheres. In what follows we shall make the following assumptions: (1) that the density of closest packing of hard spheres is equal to the density of regular close packing (this assertion has not been proven

but is widely held to be true) and (2) that the density of closest packing of HERs is equal to the density of regular close packing of spheres. This second assumption is more drastic than the former, because it is conceivable that more closely packed HER structures exist which cannot be transformed to hard-sphere structures at the same packing fraction.

As the density of the HER solid is reduced from closest packing it is possible that orientational order is destroyed before translational order disappears. In other words, the solid may undergo an orientational order-disorder transition. Whether or not this will happen depends in a subtle way on the relative stability of solid and fluid phases, and little can be said *a priori*. Only in the case of hard spheres we know for certain that the solid phase must be orientationally disordered at all densities.

The aim of the present paper is to provide numerical data on the phase diagram of HERs for $1/3 \leqslant x \leqslant 3$. Some of the results given in this paper have been reported in preliminary publications [6, 7]. The present paper contains a description of the numerical techniques, insofar as these are non-standard, a description of the method to compute the absolute free energy of both solid and nematic phases, and tables containing the equation-of-state data for all systems studied. In the following section we discuss the problem of free energy computations of molecular solids and nematics and certain technical aspects of the Monte Carlo method used. In § 3 we present the results of the simulations including tabular material. In a subsequent paper [8] a comparison is made between the simulation results and a number of model predictions.

2. Computational technique

2.1. *Monte Carlo method*

Most simulations described in the present paper were performed using the constant-pressure Monte Carlo technique [9, 10]. In a number of cases a constant volume method described in [5] was used. However, for the study of the solid phase the convential constant-P MC (and, *a fortiori* the constant-V MC) cannot be used because the shape of the crystal unit cell changes with pressure. The logical solution is to use the Monte Carlo equivalent of the molecular dynamics method developed by Parrinello and Rahman [11]. This implies that, instead of performing Metropolis sampling on the volume of the system, as in the usual constant-P MC method, the elements of the symmetrized h-matrix are sampled; $\mathbf{h}$ is the matrix which relates the real coordinates $\mathbf{r}$; to the scaled coordinates $\mathbf{s}_i$: $\mathbf{r}_i = \mathbf{h} \,.\, \mathbf{s}_i$ [12]. In our simulations the initial solid configuration had a rhombohedral structure. It was obtained by distorting an f.c.c. hard sphere lattice along the (111)-axis by an amount a/b. The periodic cell in the MC simulation was orthorhombic; one edge was initially along the (111) axis of the hard-sphere solid. During the simulation we only sampled the diagonal elements of $\mathbf{h}$ (i.e. the periodic cell was kept orthorhombic). The reason for this restricted sampling of box shapes was the following: because of the infinite degeneracy of close packed structures of HERs [13] one should expect large amplitude fluctuations of the unit cell shape which correspond to reorientations of the 'distortion axis'. By keeping $\mathbf{h}$ diagonal we suppress such fluctuations. However, we retain the possibility that the aspect ratio of the unit cell changes from the value at close packing. The rhombohedral starting structure was chosen because of its high symmetry. It

seems likely that this structure is the equilibrium structure of almost close-packed HERs or, if it is not, its free energy is probably very close to the free energy of the true equilibrium structure.

During our simulations we always found that the solid retained its rhombohedral symmetry (this was not imposed, as all three diagonal elements of **h** could be varied independently), even though the edge length and rhombohedral angle changed with pressure. We also observed that if we fixed the shape of the periodic box, we obtained almost identical compressibility data for the solid but in that case the free energy of the solid close to melting was appreciably higher than the free energy of the relaxed solid. This suggests that if the unit-cell shape is kept fixed the pressure tensor has a large traceless symmetric part in addition to the hydrostatic contribution.

The MC simulations consisted of a succession of trial moves in which we attempted to change the coordinates of the individual ellipsoids. After every sweep, i.e. after attempting to move every particle once, a box shape change was attempted. A particle move consisted of a combined translation and reorientation. The translational displacements were generated by adding random numbers in the interval $\{-\Delta, \Delta\}$ to the x, y and z coordinates of the centre of mass of a given particle. The orientational displacements were generated by adding a vector of fixed length r but with an orientation chosen at random from an isotropic distribution to the unit vector specifying the orientation of a given particle, i. The resulting vector $\mathbf{u}_i + \mathbf{r}$ was thereupon normalized to yield the new unit vector $\mathbf{u}_i'$. The magnitudes of Δ and r were chosen such that the average acceptance of a combined translation-reorientation move was $\sim$20–30 per cent. The ratio of Δ and r was fixed by the requirement that translation and reorientation contributed about equally to the probability that a move would be rejected. The criterion to decide whether or not a given move generated an acceptable configuration, i.e. one free of hard-core overlap, was taken directly from the work of Vieillard–Baron [13]. Perram *et al.*, [14] have recently developed an alternative criterion which, according to these authors is more satisfactory but, as the latter papers only appeared after we carried out our simulations we have been unable to compare the two methods. The box-shape changing moves were carried out by randomly selecting one of the three diagonal elements of **h** and changing it by a factor $\exp(\alpha x)$ where x is a random number between $-1/2$ and $1/2$ and α was chosen such that the overall acceptance of such volume changing moves was $\sim$20–30 per cent. When simulating the fluid phase all diagonal elements of **h** were scaled by the same factor; this corresponds to the usual constant pressure MC procedure [10].

2.2. *Free energy computation*

In order to locate the first order phase transitions between solid and fluid phases and between isotropic and nematic fluids one needs to know the absolute free energy of the coexisting phases. For the isotropic phase computing the free energy poses no particular problems. The excess free energy of the isotropic fluid, i.e. the difference between the free energy of an isotropic fluid of HERs at density ρ and that of an ideal gas (of linear molecules) at the same density, is given by

$$F_{\mathrm{EX}}(\rho) = \int_0^{\rho} (P(\rho') - P_{\mathrm{ID.GAS}}(\rho'))/\rho'^2 \, d\rho', \tag{2.1}$$

where $P(\rho)$ is the pressure of the system of HERs at density ρ and $P_{\text{ID.GAS}}(\rho) = \rho kT$ is the ideal gas pressure at this density. $P(\rho')$ is obtained in the course of the Monte Carlo simulation. It should be noted that the integral on the right-hand side of equation (2.1) is well-behaved at low densities because the integrand is of the form $(B_2 + B_3\rho + \ldots)$ where B_n is the nth virial coefficient of the HERs. We computed B_2 analytically and B_3 numerically [8]. The integration in equation (2.1) was performed by first fitting $P(\rho')$ to a 'generalized y-expansion' form [15]

$$P(\rho') = (6/\pi)\left(\sum_{n=1}^{N} C_n y^n\right), \tag{2.2}$$

with $y = \eta/(1-\eta)$ and $\eta = (4\pi/3)ab^2\rho'$ is the packing fraction. Barboy and Gelbart observed that for a number of hard-core fluids an N-term y-expansion tends to reproduce the true equation of state better than the corresponding N-term virial series. We found that for HERs with $1/3 \leqslant x \leqslant 3$, we could always reproduce the Monte Carlo equation of state over the entire isotropic range with at most six terms in the series of equation 2.2. Moreover, the coefficients C_1, C_2 and C_3 are known because $C_1 = B_1$ $(=1)$, $C_2 = B_2 - 1$ and $C_3 = B_3 - 2B_2 + 1$.

The absolute free energy of nematic phases cannot be determined in the above fashion because a nematic phase cannot be expanded to a dilute gas without crossing a first-order phase transition. However, in a sufficiently strong external field this first-order transition can be suppressed. We make use of this fact to devise a reversible path from the ideal gas phase to the dense nematic fluid phase. We consider a hamiltonian

$$H(\lambda) = H_0 + \lambda \sum_{i=1}^{N} \sin^2 \theta_i, \tag{2.3}$$

where H_0 is the hamiltonian of the HER system without external field, λ the strength of the external field and θ_i the angle of the axis of the i-th molecule with the direction of the field. We denote the critical field strength beyond which the first order isotropic–nematic transition disappears by λ_c. We now construct the following path from the ideal gas to nematic phase. First switch on the field at $\rho = 0$ to a value $\lambda_M > \lambda_c$; $\Delta F(0 \rightarrow \lambda_M; 0)$, the resulting increase in the free energy of the ideal gas can be computed analytically. Next we compress the HER system while keeping the external field constant to a density ρ_N, at which the system with no external field applied is well inside the nematic phase. The excess free energy of the HER fluid increases during this compression by an amount

$$\Delta F_{\text{EX}}^{\lambda_M}(\lambda_M\,;\, 0 \rightarrow \rho_N) = \int_0^{\rho_N} (P_{\lambda_M}(\rho) - P_{\text{ID.GAS}}(\rho))/\rho^2 \, d\rho, \tag{2.4}$$

where $P_{\lambda_M}(\rho)$ denotes the pressure of an HER fluid at density ρ in an applied field of strength λ_M. Once again, the low density behaviour of the integrand can be written in terms of virial coefficients

$$(P_{\lambda_M}(\rho) - P_{\text{D.GAS}}(\rho))/\rho^2 = B_2^{\lambda_M} + B_3^{\lambda_M}\rho + \ldots, \tag{2.5}$$

where $B_n^{\lambda_M}$ is the value of the nth virial coefficient in an applied field of strength λ_M. The exact expression for $B_2^{\lambda_M}$ is known (see Appendix A). As before we fit $P_{\lambda_M}(\rho)$ to an expression of the form

$$P_{\lambda_M}(\rho) = \left(\frac{6}{\pi}\right) \sum_{n=1}^{N} C_n^{\lambda_M} y^n, \tag{2.6}$$

where $C_1^{\lambda_M} = 1$ and $C_2^{\lambda_M} = B_2^{\lambda_M} - 1$. Typically a five-term power series in y accurately reproduces the MC data. Finally we slowly switch off the external field at constant density. The free energy change per particle in the last step is equal to

$$\Delta F(\lambda_M \to 0;\, \rho_N) = -\int_0^{\lambda_M} \left(\frac{\partial F}{\partial \lambda}\right)_{\rho_N} d\lambda = -\int_0^{\lambda_M} \left\langle \frac{\partial H}{\partial \lambda} \right\rangle_{\rho_N} d\lambda$$
$$= -N^{-1} \int_0^{\lambda_M} \sum_{i=1}^{N} \langle \sin^2 \theta_i \rangle_{\lambda, \rho_N} d\lambda. \tag{2.7}$$

In the simulations presented here we found it more convenient to switch off the field at constant pressure rather than at constant density. As $\langle \partial H/\partial \lambda \rangle_P = (\partial G/\partial \lambda)_P$, we then measure a free enthalpy difference rather than a free energy difference. But this is immaterial since knowledge of one suffices to determine the other.

The free energy of the solid phase is computed in a similar way. We construct a reversible path from the solid structure under consideration to an Einstein crystal of the same structure [16]. To this end we modify the hamiltonian H_0 of the HER system by including 'external fields' which, in the limit of large coupling constant, contrain the solid to approach a molecular Einstein crystal

$$H(\lambda_1, \lambda_2) = H_0 + \lambda_1 \sum_{i=1}^{N} (\mathbf{r}_i - \mathbf{r}_i^0)^2 + \lambda_2 \sum_{i=1}^{N} \sin^2 \theta_i. \tag{2.9}$$

In equation (2.9) $\mathbf{r}_i - \mathbf{r}_i^0$ is the displacement of molecule i from its average position, θ_i is the angle of the axis of the ith molecule with the direction of the aligning field. In the limit of large coupling constants (λ_1, λ_2) the partition function corresponding to the above hamiltonian can be evaluated analytically, provided that the probability of hard-core overlaps vanishes in the limit $\lambda_1, \lambda_2 \to \infty$

$$Q(\lambda_1, \lambda_2) \xrightarrow[\substack{\lambda_1 \to \infty \\ \lambda_1 \to \infty}]{} N^{-3/2} (\pi/\beta\lambda_1)^{3/2(N-1)} (2\pi/\beta\lambda_2)^N. \tag{2.10}$$

At finite values of λ_1, λ_2 the expression for the partition function of a perfect Einstein crystal is still known in closed form. Corrections to the partition function due to hard-core overlaps can be computed in a systematic way using a cluster expansion [16] or numerically by performing umbrella sampling of the system with the full hamiltonian from configurations of the corresponding ideal Einstein crystal. The free energy of the solid without external fields is then obtained by integrating $(\partial F/\partial \lambda_1) = \sum_i \langle (r_i - r_i^0)^2 \rangle_{\lambda_1, \lambda_2}$ and $(\partial F/\partial \lambda_2) = \sum_i \langle \sin^2 \theta_i \rangle_{\lambda_1, \lambda_2}$ along some conveniently chosen path. Such a path is described by a set of equations of the form: $\lambda_1 = f_1(\xi)$, $\lambda_2 = f_2(\xi)$ such that for $\lambda_1 = \lambda_2 = 0$ for $\xi = 0$ and $\lambda_1 = \lambda_1^{\max}$ and $\lambda_2 = \lambda_2^{\max}$ for $\xi = 1$. With these definitions the expressions for the free energy of the solid without external fields becomes

$$F(\lambda_1 = 0, \lambda_2 = 0) = F(\lambda_1 = \lambda_1^{\max}, \lambda_2 = \lambda_2^{\max})$$
$$- \int_0^1 d\xi \left[\left(\frac{\partial F}{\partial \lambda_1}\right)\left(\frac{\partial \lambda_1}{\partial \xi}\right) + \left(\frac{\partial F}{\partial \lambda_2}\right)\left(\frac{\partial \lambda_2}{\partial \xi}\right) \right]. \tag{2.11}$$

In our calculation we always used the parametrization $\lambda_1 = \lambda_1^{\max}\xi$ and $\lambda_2 = \lambda_2^{\max}\xi$. One point requires special attention. The free energy computations are necessar-

ily carried out at constant volume and fixed box shape. Without these constraints hard core overlaps cannot be eliminated by increasing λ_1 and λ_2. It is very important that the box shape chosen for the free energy integration is indeed the one corresponding to the equilibrium shape of the crystal unit cell at that particular density. Otherwise one would end up computing the free energy of a strained crystal which is, of course, higher than the free energy of the unstrained solid. We found this effect to be quite appreciable. Once the free energy of the solid had been determined at one particular density and, where applicable, also the free energy of one nematic state point, the coexistence points were determined as follows. The equation of state for all 3 (or 2) branches was fitted to an expression of the form given in equation (2.2) above, where we made use of our knowledge of the first 3 virial coefficients to fix the first three coefficients in the isotropic case. Once the dependence of P on ρ is given, the computation of F and hence $\mu N = F + PV$ at any density is straightforward. The points where the pressure and chemical potential of two phases are equal were determined numerically.

3. Results

Figures 1 and 2 show the Monte Carlo equation-of-state data for hard ellipsoids of revolution with length-to-breadth ratios $x = 3$, 2·75, 2, 1·25, 0·8, 0·5, 1/2·75 and 1/3. The data displayed in figures 1 and 2 have been collected in tables 1, 2 and 3. The length of the individual Monte Carlo runs was between 10^4 and 2×10^4 attempted moves per particle, excluding equilibration. For a number of state points several independent runs were carried out. The scatter in the results for such simulations is a direct measure for the estimated error in the equation-of-state data. Typically we find a relative error in the density (or pressure) of the order of 1 per cent but in the vicinity of phase transitions the error tends to be somewhat larger. For systems with x in the interval $2 \geqslant x \geqslant \frac{1}{2}$ we observe a phase diagram consisting of an isotropic fluid branch at low densities and a solid branch at high densities. As we go to the less spherical systems $x \geqslant 2{\cdot}75$, $x \leqslant 1/2{\cdot}75$, a nematic fluid branch appears in addition to the isotropic fluid and crystalline solid branches. This nematic branch is more clearly visible in figure 3. The onset of orientational order was studied by monitoring the behaviour of the orientational correlation function $g_2(\mathbf{r}_1 - \mathbf{r}_2) \equiv \langle P_2(\mathbf{1}(\mathbf{r}_1) \cdot \mathbf{1}(\mathbf{r}_2))\rangle$, where P_2 stands for the second Legendre polynomial and $\mathbf{1}(\mathbf{r})$ is the unit vector characterizing the orientation of a molecule at a position $\mathbf{r}$. In the isotropic phase $g_2(r)$ decays to zero within approximately one molecular diameter. In the nematic phase $g_2(r)$ approaches a constant value at large r

$$g_2(r) \xrightarrow[r \to \infty]{} \langle P_2 \rangle^2, \tag{3.1}$$

where $\langle P_2 \rangle$ is the average value of the nematic order parameter. In our simulations we observe that $g_2(r)$, which is initially short ranged, becomes long ranged as the density is increased. Upon reducing the density, $g_2(r)$ once more becomes short ranged. This behaviour is illustrated in figure 4. It is important to note that the isotropic–nematic transition exhibits hysteresis. The isotropic fluid can be overcompressed and the nematic fluid can be overexpanded. This effect is more pronounced for prolate than for oblate ellipsoids. Hysteresis effects are clearly visible in figures 3 and 4. As a consequence the isotropic–nematic point cannot be

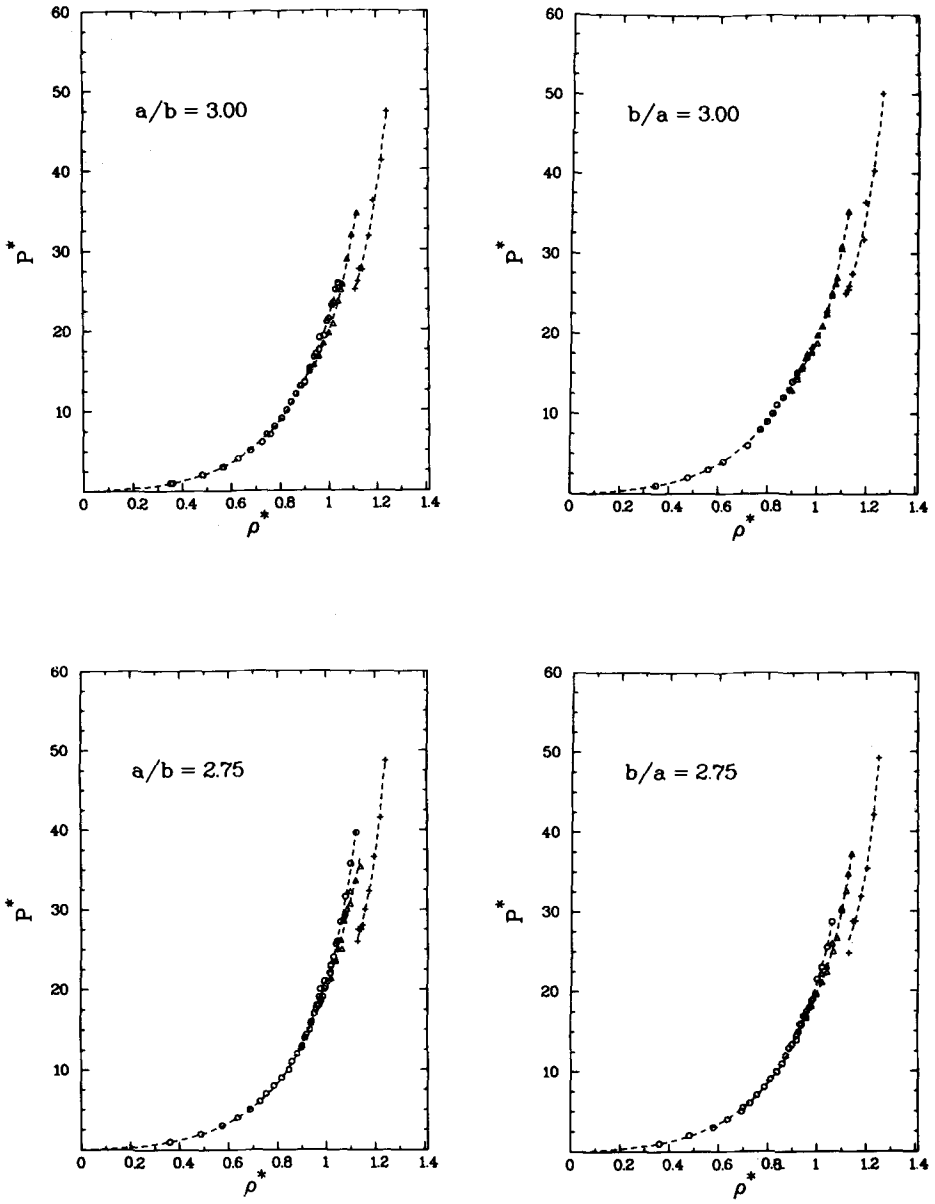

Figure 1. Equation of state data of hard ellipsoids of revolution with length-to-breadth ratios $x = 3$, 2·75, 1/2·75 and 1/3. The pressure is in units $kT/8ab^2$, the density in units $(8ab^2)^{-1}$. Open circles: isotropic branch, open triangles: nematic branch, pluses: solid branch. The data points have been tabulated in tables 1–3, the parameters describing the fits through the data (dashed curves) have been collected in table 6.

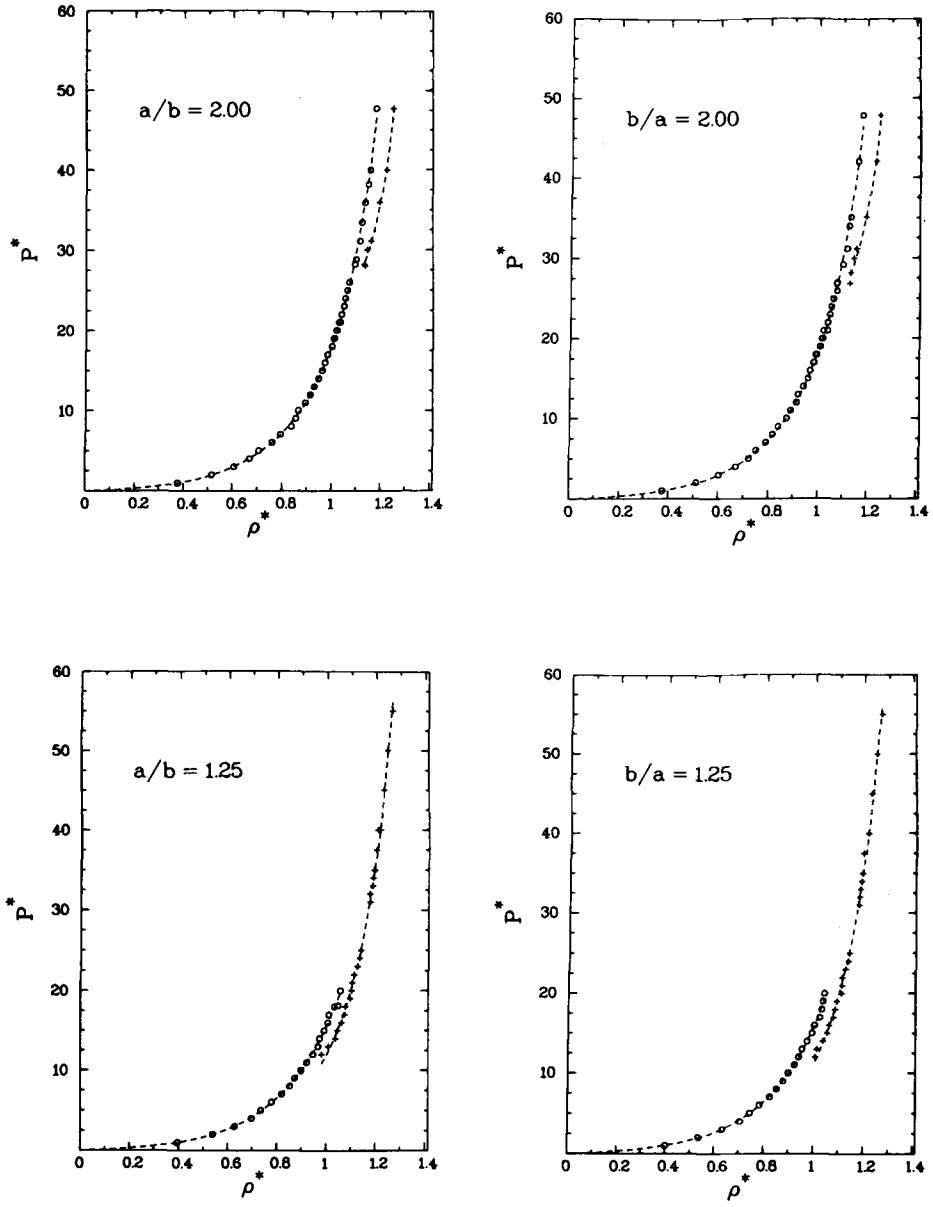

Figure 2. Equation of state data of hard ellipsoids of revolution with length-to-breadth ratios $x = 2$, 1·25, 0·8 and 0·5. The units are as in figure 1. Open circles: isotropic fluid branch, pluses: solid branch. The data points have been tabulated in tables 1 and 3, the parameters describing the fits through the data (dashed curves) have been collected in table 6.

Table 1. Equation of state data for the isotropic fluid phase of hard ellipsoids of revolution with length-to-breadth ratio $x = 3$, 2·75, 2, 1·25, 0·8, 0·5, 1/2·75 and 1/3. Constant-P and constant-V MC data in the table can be distinguished because for the former the pressure is always a round number. The unit of density is $(8ab^2)^{-1}$, the unit of pressure is $kT/(8ab^2)$.

$x = 3$		$x = 1/3$		$x = 2{\cdot}75$		$x = 1/2{\cdot}75$	
P	ρ	P	ρ	P	ρ	P	ρ
1·000	0·352	1·000	0·349	1·000	0·362	1·000	0·360
1.000	0·360	2·000	0·479	2·000	0·488	2·000	0·482
2·000	0·484	3·000	0·563	3·000	0·576	3·000	0·581
2·000	0·481	4·000	0·624	4·000	0·639	4·000	0·639
3·000	0·565	6·000	0·724	5·000	0·689	5·000	0·695
3·000	0·569	8·000	0·772	6·000	0·729	5·000	0·700
4·000	0·628	9·000	0·801	7·000	0·755	6·000	0·728
5·000	0·681	10·000	0·823	8·000	0·787	7·000	0·756
5·000	0·680	11·000	0·839	9·000	0·816	8·000	0·787
6·000	0·728	12·000	0·865	10·000	0·847	9·000	0·810
7·000	0·759	13·000	0·890	11·000	0·859	10·000	0·837
7·000	0·746	14·043	0·900	12·000	0·881	11·000	0·858
8·000	0·777	14·000	0·900	12·757	0·900	12·000	0·874
9·000	0·805	15·000	0·918	13·000	0·903	13·000	0·888
9·000	0·806	15·165	0·920	14·000	0·914	13·441	0·900
10·000	0·826			14·469	0·920	13·408	0·900
11·000	0·845			15·000	0·936	14·000	0·919
11·000	0·846			15·817	0·940	14·634	0·920
12·000	0·866			16·000	0·945	14·535	0·920
13·000	0·886			17·000	0·954	15·000	0·927
13·000	0·882			17·511	0·960	16·000	0·934
13·374	0·900			18·000	0·972	15·967	0·940
13·483	0·900			18·000	0·963	15·848	0·940
13·449	0·900			18·419	0·980	17·000	0·958
15·227	0·920			18·759	0·980	17·000	0·945
15·175	0·920			19·000	0·974	17·564	0·960
14·827	0·920			19·000	0·988	18·000	0·970
15·000	0·922			20·000	0·979	18·000	0·972
16·593	0·940			20·000	0·995	18·000	0·980
17·000	0·947			20·282	1·000	19·000	0·985
17·470	0·960			21·000	1·994	21·483	1·000
19·000	0·960			21·000	1·009	23·012	1·020
19·215	0·980			22·000	1·015	25·523	1·040
21·000	0·994			22·000	1·018	28·706	1·060
21·322	1·000			22·881	1·020		
23·000	1·012			23·000	1·020		
23·294	1·020			24·000	1·029		
25·000	1·029			25·656	1·040		
25·833	1·040			26·000	1·046		
				28·437	1·060		
				31·527	1·080		
				35·723	1·100		
				39·658	1·125		

Table 1 (*continued*).

$x = 3$		$x = 1/3$		$x = 2{\cdot}75$		$x = 1/2{\cdot}75$	
P	ρ	P	ρ	P	ρ	P	ρ
1·000	0·377	1·000	0·3760	1·000	0·395	1·000	0·401
2·000	0·517	2·000	0·5120	2·000	0·539	2·000	0·536
3·000	0·608	3·000	0·6040	3·000	0·630	3·000	0·634
4·000	0·671	4·000	0·6710	4·000	0·699	4·000	0·706
5·000	0·709	5·000	0·7230	5·000	0·737	5·000	0·745
6·000	0·760	6·000	0·7520	6·000	0·780	6·000	0·784
7·000	0·794	7·000	0·7900	7·000	0·821	7·000	0·825
8·000	0·838	8·000	0·8170	8·000	0·854	8·000	0·852
9·000	0·855	9·000	0·8390	9·000	0·874	9·000	0·879
10·000	0·866	10·000	0·8730	10·000	0·900	10·000	0·900
11·000	0·894	11·000	0·8900	11·000	0·923	11·000	0·924
12·000	0·914	12·000	0·9130	12·000	0·947	12·000	0·941
13·000	0·930	13·000	0·9190	13·000	0·968	13·000	0·955
14·000	0·948	14·000	0·941	14·000	0·974	14·000	0·975
15·000	0·963	15·000	0·959	15·000	0·993	15·000	0·995
16·000	0·974	16·000	0·968	16·000	1·008	16·000	1·004
17·000	0·984	17·000	0·984	17·000	1·012	17·000	1·026
17·000	0·986	17·000	0·982	18·000	1·035	18·000	1·034
18·000	1·001	18·000	0·990	18·123	1·050	19·000	1·039
18·000	1·001	18·000	0·996	20·000	1·059	20·000	1·045
19·000	1·008	19·000	1·005				
19·000	1·013	19·000	1·009				
20·000	1·023	20·000	1·012				
20·000	1·019	20·000	1·017				
21·000	1·029	21·000	1·037				
21·000	1·036	21·000	1·020				
22·000	1·040	22·000	1·036				
22·000	1·041	22·000	1·038				
23·000	1·050	23·000	1·046				
23·000	1·052	24·000	1·052				
24·000	1·056	25·000	1·060				
25·000	1·065	26·000	1·075				
26·000	1·073	26·870	1·074				
28·220	1·096	27·000	1·076				
28·797	1·100	29·222	1·100				
31·080	1·117	31·180	1·117				
33·415	1·125	34·034	1·125				
35·890	1·138	35·130	1·132				
39·960	1·1580	42·080	1·160				
38·167	1·150	47·850	1·178				
47·720	1·184						

extracted directly from the equation of state data. This holds, *a fortiori*, for the location of the solid–liquid coexistence point. The density jump from solid to liquid is typically of the order of 6–8 per cent as compared with 1–2 per cent for the isotropic–nematic transition. In fact, spontaneous crystallization of the overcompressed fluid was hard to achieve. We only observed it in the overcompressed fluid phase of ellipsoids with $a/b = 1{\cdot}25$ and $0{\cdot}8$. In the vicinity of the isotropic–nematic transition very large and sluggish fluctuations in the nematic order parameter are observed both in the isotropic and in the nematic phase. Typical

Table 2. Equation of state data for the nematic fluid phase of hard ellipsoids of revolution with length-to-breadth ratios $x = 3$, 2·75, 1/2·75 and 1/3. Most runs were at constant volume; constant-P runs are easily recognized by the fact that the pressure is a round number. Units as in table 1.

$x = 3$		$x = 2{\cdot}75$		$x = 1/2{\cdot}75$		$x = 1/3$	
P	ρ	P	ρ	P	ρ	P	ρ
15·6602	0·940	21·3630	1·020	17·1150	0·960	12·9580	0·900
16·7127	0·960	22·4802	1·020	16·7325	0·960	14·3460	0·920
18·3252	0·980	23·4760	1·040	18·2150	0·980	14·7310	0·920
19·5922	1·000	23·6329	1·040	18·2439	0·940	15·6780	0·940
20·7425	1·020	25·0000	1·064	19·7830	1·000	15·9270	0·940
23·5652	1·040	25·0000	1·047	19·6489	1·000	16·0110	0·940
25·0000	1·053	26·1230	1·060	21·1220	1·020	16·0000	0·943
25·6909	1·060	28·5070	1·075	22·1896	1·020	17·0000	0·954
28·8181	1·080	29·2230	1·075	23·1310	1·040	17·0870	0·960
31·8018	1·100	29·4317	1·080	22·3931	1·040	17·3690	0·960
34·4831	1·120	30·0000	1·086	25·0000	1·065	17·5930	0·960
		32·2151	1·100	25·9890	1·060	17·6700	0·980
		30·7013	1·100	26·6520	1·080	17·8690	0·980
		33·6447	1·120	30·1607	1·100	18·4530	0·980
		35·3705	1·140	30·4810	1·000	18·8590	1·000
				32·6169	1·120	19·8540	1·000
				34·7430	1·125	20·9410	1·020
				37·2378	1·140	20·9830	1·020
						22·4850	1·040
						22·9770	1·040
						24·7900	1·060
						25·0960	1·060
						26·2596	1·075
						26·9800	1·080
						30·6355	1·100
						30·9180	1·100
						35·2853	1·250

examples are shown in figure 5. The order parameter in figure 5 is defined as $-2\lambda_0$, where λ_0 is the middle eigenvalue of the tensor order parameter $Q_{\alpha\beta}$ (for a discussion, see [5]). Because of these large fluctuations our statistics on the nematic order parameters were poor and hence no detailed study of the density dependence of the order parameter was attempted. In order to locate the thermodynamic phase transitions the absolute free energy of the coexisting phases needs to be determined. To this end we employ the methods described in § 2. The essence of the techniques described in § 2 is that a reversible path is constructed which links the thermodynamic phase under consideration to a state of known free energy.

For the isotropic phase the reference state is the ideal gas. The reference state for the nematic is an ideal gas in a 'field' of strength λ_M. For sufficiently high values of λ_M we first reversibly compress the system at constant λ_M and *then* reversibly switch off the field. We do not know *a priori* how large λ_M should be chosen to ensure that such a path is indeed reversible. Our experience is that a field strength $\lambda_M = 5$ (in units kT) is sufficiently high to avoid the first order

Table 3. Equation of state data for the solid phase of hard ellipsoids of revolution with length-to-breadth ratios $x = 3$, 2·75, 1·25, 0·8, 0·5, 1/2·75 and 1/3. These simulations were carried out at constant pressure, with a fluctuating box shape, as described in the text. The units are as in table 1. For $x = 1{\cdot}25$ and $x = 0{\cdot}8$ a orientational order-disorder transition takes place at $\rho = 1{\cdot}20$.

$x = 3$		$x = 1/3$		$x = 2{\cdot}75$		$x = 1/2{\cdot}75$	
P	ρ	P	ρ	P	ρ	P	ρ
25·0000	1·111	25·0000	1·115	26·0000	1·127	24·8000	1·128
26·0000	1·123	25·5300	1·123	27·5000	1·130	28·7600	1·145
27·5000	1·144	25·5300	1·124	27·4800	1·139	28·7600	1·146
27·5000	1·134	25·5300	1·126	27·4800	1·141	28·7600	1·145
27·5200	1·129	26·0000	1·130	27·4800	1·135	28·7600	1·155
27·5200	1·138	27·5000	1·144	28·0000	1·149	31·8700	1·179
31·6800	1·173	27·5000	1·142	30·0000	1·159	35·3700	1·204
36·0900	1·188	31·7300	1·190	32·2900	1·177	42·0900	1·231
41·1300	1·223	36·3800	1·195	36·6200	1·195	49·2200	1·254
47·2800	1·241	40·3500	1·229	41·5500	1·222		
		50·0800	1·263	48·7000	1·245		
$x = 2$		$x = 1/2$		$x = 1{\cdot}25$		$x = 1/1{\cdot}25$	
28·0000	1·137	26·8700	1·127	12·0000	0·9819	12·0000	1·008
28·2200	1·134	28·2200	1·131	13·0000	1·010	13·0000	1·014
30·0000	1·146	30·0000	1·144	14·0000	1·039	14·0000	1·039
31·0800	1·162	31·1800	1·155	15·0000	1·048	15·0000	1·056
35·8900	1·198	35·1300	1·195	16·0000	1·065	16·0000	1·064
39·9600	1·226	42·0800	1·234	17·0000	1·077	17·0000	1·081
47·7200	1·254	47·8500	1·250	18·0000	1·080	18·0000	1·088
				19·0000	1·099	19·0000	1·095
				20·0000	1·105	20·0000	1·114
				21·0000	1·108	21·0000	1·116
				22·0000	1·116	22·0000	1·117
				23·0000	1·127	23·0000	1·128
				24·0000	1·135	24·0000	1·139
				25·0000	1·141	25·0000	1·143
				31·0000	1·178	31·0000	1·180
				32·0000	1·176	32·0000	1·183
				33·0000	1·188	33·0000	1·187
				34·0000	1·190	34·0000	1·192
				35·0000	1·198	35·0000	1·197
				35·0000	1·193	35·0000	1·195
				37·5000	1·201	37·5000	1·198
				40·0000	1·206	40·0000	1·218
				40·0000	1·216	40·0000	1·216
				45·0000	1·232	45·0000	1·230
				50·0000	1·247	50·0000	1·253
				55·0000	1·266	55·0000	1·271

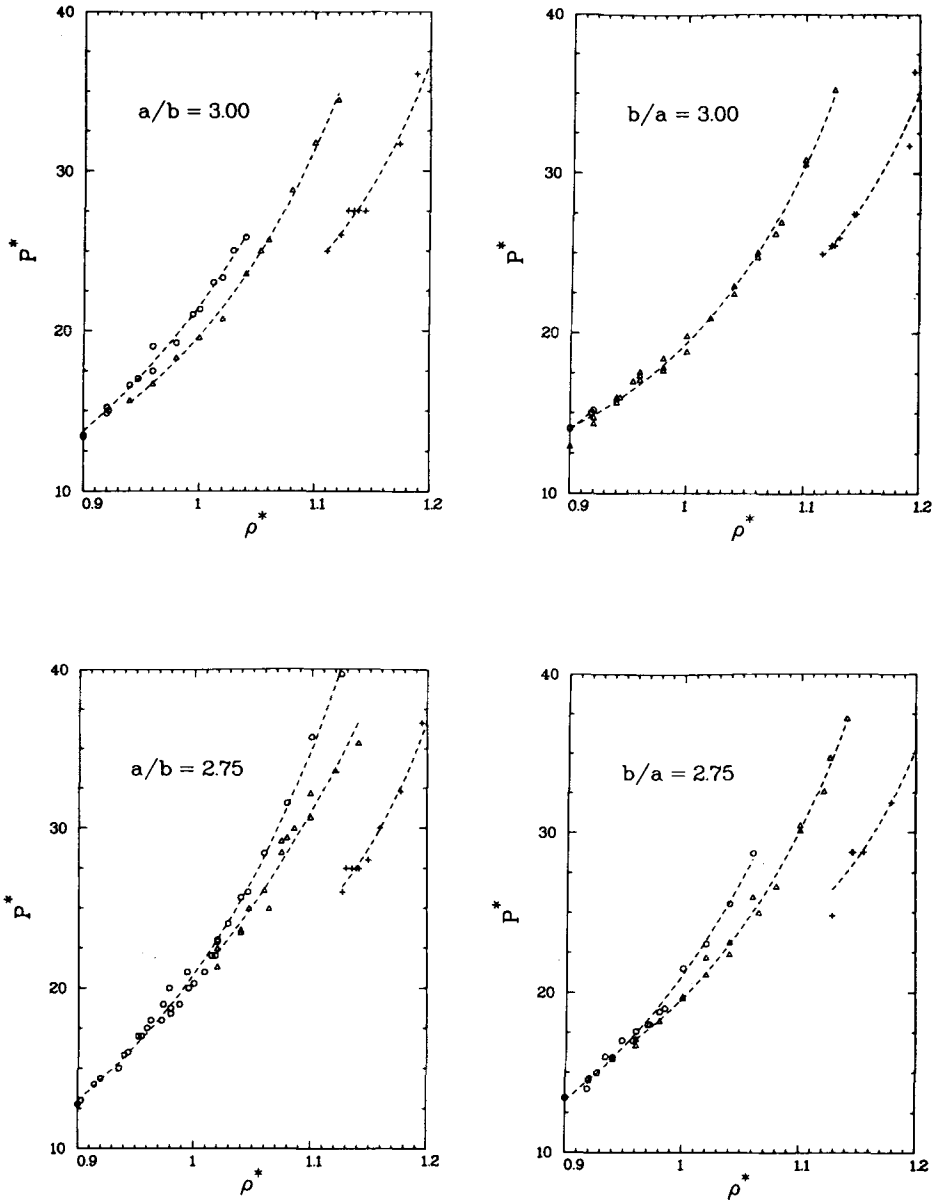

Figure 3. Equation of state of hard ellipsoids of revolution with length-to-breadth ratios 3, 2·75, 1/2·75 and 1/3, in the density range where a nematic branch is observed. Meaning of symbols as in figure 1.

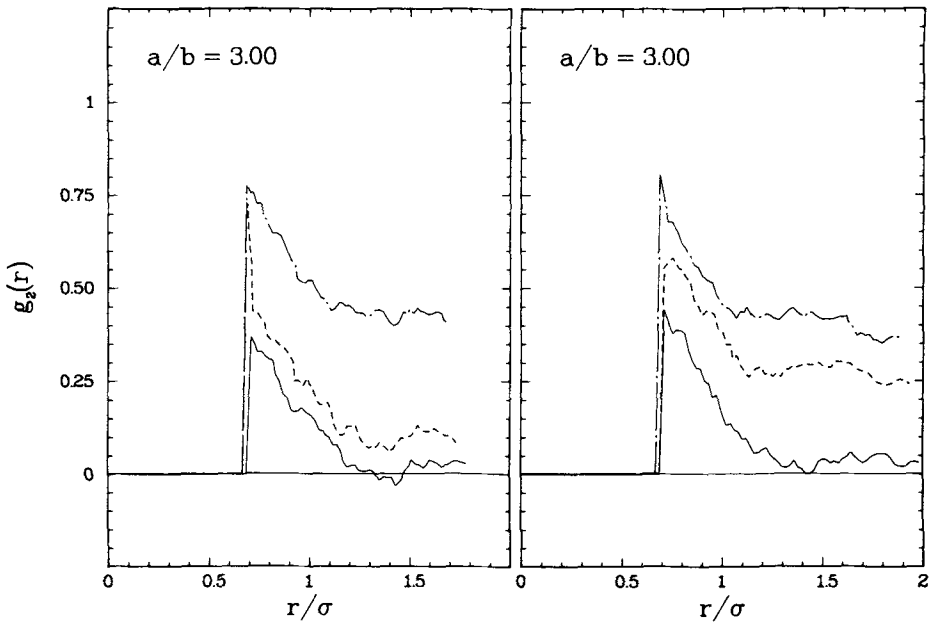

Figure 4. Example of the behaviour of the orientational correlation function $g_2(r) \equiv \langle P_2(1(0) \cdot 1(r)) \rangle$, at densities $\rho = 0{\cdot}92$ (drawn curve), $\rho = 1{\cdot}00$ (dashed curve) and $\rho = 1{\cdot}08$ (dash–dot). The left hand figure shows the behaviour of $g_2(r)$ on compression, the right hand figure shows the behaviour on expansion. The length-to-breadth ratio, in this figure is $a/b = 3$.

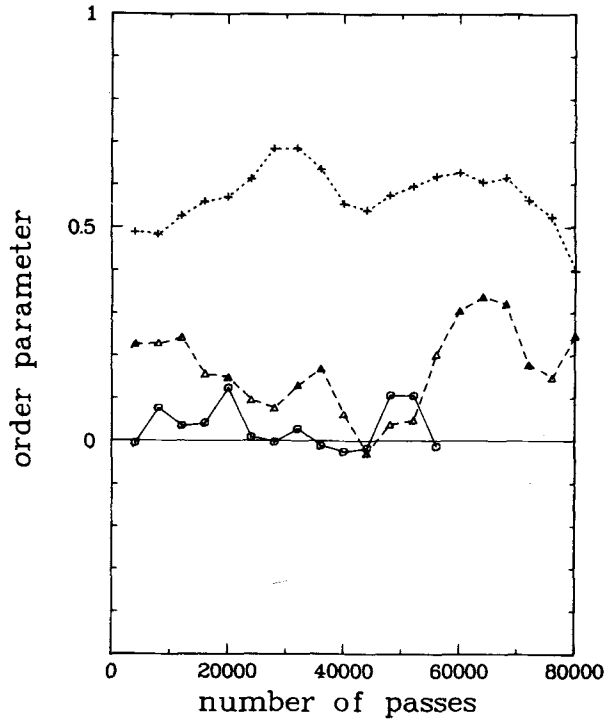

Figure 5. Slow fluctuations in the nematic order parameter of hard ellipsoids of revolution. Pluses: $b/a = 3$, $\rho = 0{\cdot}98$ (nematic); open triangles: $b/a = 3$, $\rho = 0{\cdot}92$ (super expanded nematic); open squares: $a/b = 3$, $\rho = 0{\cdot}90$ (isotropic).

Table 4. Equation of state data of a fluid of hard ellipsoids of revolution under the influence of an external perturbation $\lambda \sum_i \sin^2 \theta_i$ (see equation (2.3)), with $\lambda = 5$ (in units kT) for $x = 3$, 2·75, 1/2·75 and 1/3. All runs were carried out at constant pressure. For $x = 3$ data were shown for a system of $N = 90$ ellipsoids ($P = 1$ to 12, upper part) and $N = 108$ ellipsoids ($P = 1$ to 25, lower part). No systematic system-size dependence was observed. Units as in table 1.

$x = 3$		$x = 2{\cdot}75$		$x = 1/2{\cdot}75$		$x = 1/3$	
P	ρ	P	ρ	P	ρ	P	ρ
1·000	0·374	1·00	0·378	1·00	0·379	1·000	0·377
2·000	0·510	2·00	0·512	2·00	0·512	2·000	0·501
3·000	0·593	3·00	0·598	3·00	0·600	3·000	0·595
4·000	0·652	5·00	0·719	5·00	0·718	4·000	0·650
5·000	0·712	7·00	0·802	7·00	0·786	5·000	0·706
6·000	0·759	9·00	0·849	9·00	0·841	6·000	0·754
7·000	0·785	11·00	0·891	11·00	0·902	7·000	0·785
8·000	0·823	13·00	0·937	13·00	0·927	8·000	0·815
9·000	0·858	15·00	0·966	15·00	0·960	9·000	0·846
10·000	0·863	17·00	0·987	17·00	1·004	10·000	0·869
11·000	0·899	19·00	1·016	19·00	1·021	11·000	0·891
12·000	0·908	21·00	1·037	21·00	1·043	12·000	0·908
1·000	0·372	23·00	1·530	23·00	1·060	13·000	0·938
2·000	0·504	25·00	1·079	25·00	1·085	14·000	0·953
3·000	0·602					15·000	0·968
5·000	0·709					16·000	0·980
7·000	0·794						
9·000	0·842						
11·000	0·891						
13·000	0·939						
15·000	0·962						
17·000	0·991						
19·000	1·009						
21·000	1·038						
23·000	1·064						
25·000	1·080						

transition. Table 4 contains the equation of state of HERs with $x = 3$, 2·75, 1/2·75 and 1/3 at $\lambda_M = 5$. The different contributions to the Gibbs free energy of the nematic phase have been collected in table 5. Note that the estimated error in the absolute free energy of the nematic phase is relatively large. This is due to the fact that it is difficult to obtain good statistics on the free enthalpy change along the reversible path linking the nematic phases with and without applied field λ_M. The values given in table 5 were obtained by averaging the results of one set of runs in which the field was switched off and one set of runs in which the field was switched on. Both sets consisted of 10 runs of 10^4 passes each. All Monte Carlo equation of state data were fitted to an expression of the form

$$P(y) = (6/\pi) \sum_{n=1}^{m} c_n y^n. \tag{2.2}$$

The number of terms in the fit, m, was fixed by the requirement that increasing m did not substantially lower the χ^2 of the fit. The coefficients of all fits to the MC

Table 5. Contributions to the absolute free energy of (i) a nematic state point of HERs with $x = 3$, 2·75, 1/2·75 and 1/3 (upper part), and (ii) a solid state point of HERs with $x = 3$, 2·75, 2, 1·25, 0·8, 0·5, 1/2·75 and 1/3 (lower part). Meaning of symbols: (i) upper part-F_{ROT}: orientational contribution to the free energy (in units kT) of a gas of linear molecules at $\rho = 0$ and $\lambda = 5$ (at $\lambda = 0$, $F_{ROT} = -\ln 2$). ΔF_{EX}: the increase in the excess free energy of a gas of HERs upon compression from zero density to density ρ (column 4), corresponding to a pressure P (column 3). The free enthalpy at this pressure, $G(\lambda; P)$, is given in column 5. The change in free enthalpy caused by switching off the perturbation $\lambda = 5 \rightarrow 0$, is shown in column 6. $G(\lambda = 0; P)$ (column 7) is the resulting value for the free enthalpy of the nematic phase at pressure P. (ii) lower part-λ_M maximum value of λ_1 and λ_2 in equation (2.11). $F_{EINST}(\lambda_M)$: free energy per particle of an N-particle, fixed centre-of-mass, interacting Einstein crystal (see [16]): $F^{N}_{EINST}(\lambda_M) = F^{\infty}_{EINST}(\lambda_M) - (3/2N) \ln (\beta\lambda_M/\pi N) + \Delta F_u$, where ΔF_u is the free energy difference between the interacting and non-interacting Einstein crystal; this (very small) term was obtained by umbrella sampling. ΔF is the Monte Carlo value for the free energy difference between the interacting Einstein crystal and the fixed centre-of-mass HER solid at the same density and box shape, but at $\lambda_1 = \lambda_2 = 0$. $F(\rho)$ is the free energy of the unconstrainted HER solid at density ρ; $(F(\rho) = F_{EINST}(\lambda_M) - \Delta F - (\ln V)/N$. R is the relative compression (expansion) of the equilibrium rhombohedral crystal unit cell along its three-fold symmetry axis referred to the shape at close packing. The last column contains the number of particles, N, for which the free energy computation was performed.

a/b	$F_{ROT}(\lambda = 5; \rho = 0)$	ΔF_{EX}	P	ρ	$G(\lambda; P)$	ΔG	$G(\lambda = 0; P)$
3	1·46356	8·205	25	1·0794	31·905	0·567 ± 0·16	31·338
2·75	1·46356	7·977	25	1·0755	31·759	0·749 ± 0·18	31·010
1/2·75	1·46356	8·168	25	1·0838	31·779	0·627 ± 0·06	31·152
1/3	1·46356	6·632	16	0·9830	23·355	0·854 ± 0·16	22·502

a/b	λ_M	$F_{EINST}(\lambda_M)$	ΔF	$F(\rho)$	ρ	R	N
3	8095·69	20·7282	10·409 ± 0·02	10·2711	1·165	0·917	90
2.75	8095·69	20·7248	10·453 ± 0·02	10·2233	1·170	0·951	90
2	22019·08	23·2095	12·001 ± 0·02	11·1612	1·240	0·949	90
1·25	8095·69	20·7301	15·901 ± 0·05	4·782	1·050	0·800	96
1/1·25	22019·08	23·2157	18·252 ± 0·06	4·917	1·060	1·250	96
1/2	22019·08	23·2242	12·165 ± 0·02	11·0177	1·230	1·065	108
1/2·75	8095·69	20·7368	10·020 ± 0·01	10·6748	1·180	1·100	108
1/3	8095·69	20·7366	10·056 ± 0·01	10·6385	1·170	1·090	108

data have been collected in table 6. Equation (2.2) provides a convenient parametrization of the MC data in the density range which we studied. However, the values of the individual higher order coefficients in equation (2.2) have little physical significance because these coefficients tend to change appreciable as the number of terms, m, in equation (2.2) is varied. The free energy of the solid phase is obtained by constructing a reversible path to a molecular Einstein crystal (see §2). This involves simultaneously switching on a translational ordering field λ_1 ('harmonic springs') and an orientational ordering field λ_2 (see equation (2.9)). We chose the maximum values of λ_1 and λ_2 sufficiently high to guarantee that corrections to the free energy of the perfect Einstein crystal due to the hard-core

Table 6. Coefficients for the generalized y-expansion (equation (2.2)) fits to the Monte Carlo equation of state data. C_n^I refers to the isotropic fluid branch; C_1^I and C_2^I are known exactly, C_3^I was computed from our knowledge of B_3, C_4^I and C_5^I are parameters that yield the best fit to the MC data in table 1. C_n^N refers to the nematic fluid branch; all three coefficients were determined by fitting the MC data. C_n^S refers to the solid phase; all three coefficients were obtained by fitting the MC data. C_n^λ refers to the HER fluid in an external field $\lambda = 5$ (table 4). C_1^λ and C_2^λ are known exactly; C_3^λ and C_4^λ are best fit values.

	$x = 3$	$x = 1/3$	$x = 2{\cdot}75$	$x = 1/2{\cdot}75$	$x = 2$	$x = 1/2$	$x = 1{\cdot}25$	$x = 1/1{\cdot}25$
C_1^I	1	1	1	1	1	1	1	1
C_2^I	4·454	4·454	4·211	4·211	3·538	3·538	3·053	3·053
C_3^I	5·944	6·832	5·392	6·069	4·018	4·180	3·073	3·141
C_4^I	−3·019	−3·955	−3·273	−3·947	−1·616	−1·688	0·242	−0·787
C_5^I	0·825	0·921	1·464	1·594	0·642	0·693	−0·723	0·238
C_1^N	8·676	14·426	−32·367	12·780				
C_2^N	−7·385	−16·433	58·818	−12·714				
C_3^N	7·299	10·657	19·214	8·736				
C_1^S	21·191	18·848	27·168	31·596	27·695	29·917	4·082	−0·367
C_2^S	−20·918	−17·141	−28·735	−32·896	−25·997	−28·990	−3·817	1·972
C_3^S	8·964	7·349	11·478	12·233	9·576	10·602	4·763	2·845
C_1^λ	1	1	1	1				
C_2^λ	3·895	3·895	3·740	3·740				
C_3^λ	3·781	4·466	3·503	4·052				
C_4^λ	−1·085	−1·891	−0·693	−1·287				

interactions were negligible. We observed that the absolute free energy of the solid phase was rather sensitive to the shape of the crystal unit cell. The unit cell dimensions used in the free energy calculation at a given density corresponded to those obtained by averaging the fluctuating box shape in the constant-P Monte Carlo simulations (see § 2). The equilibrium shape of the unit cell at finite pressure is, in general, not the same as that at close packing, although the rhombohedral symmetry is maintained. We find that the distortion is always in the direction of cubic symmetry, i.e. as the density is lowered the particles pack as if they were less anisometric. The change in the aspect ratio of the crystal unit cell at the density where the free energy calculation was performed, referred to the aspect ratio at close packing, is given for all crystals in table 5. Note that for the systems with $x = 1{\cdot}25$ and $x = 0{\cdot}8$ the crystal close to melting is face centred cubic. Also shown in table 5 are the values of λ_1 and λ_2 used in the computation, the absolute free energy of the Einstein crystal for this value λ_1 and λ_2 and the free energy difference between the Einstein crystal and the unperturbed crystal. To evaluate the integral in equation (2.11) we used a 10-point Gauss–Legendre quadrature. In order to make the integrand a slowly varying function of the integration variable, we employed the same transformation as described in [16]. As we now know the absolute free energy of the isotropic fluid, the solid and, where applicable the nematic phases, the location of the phase transitions is straightforward. Using the y-expansion fits to the equation of state data we can compute the pressure and free energy, and hence the chemical potential, at any density. We use an iterative numerical procedure to locate the points where the pressure and chemical potential of two phases are simultaneously equal. The

Table 7. Coexistence points in the phase diagram of hard ellipsoids of revolution. The first four columns give the coexisting densities, the pressure and the chemical potential at the isotropic–nematic transition. Columns 5 to 8 give the same information for the fluid–solid transition. The number of particles is given in column 9.

a/b	ρ_{ISO}	ρ_{NEM}	P_{IN}	μ_{IN}	ρ_{FL}	ρ_{SOL}	P_{FS}	μ_{FS}	N
3	0·969	0·988	18·69	25·15	1·096	1·163	30·84	36·75	90
2·75	1·072	1·089	30·00	35·68	1·118	1·182	33·36	38·73	90
2	—	—	—	—	1·185	1·252	46·97	49·03	90
1·25	—	—	—	—	0·983	1·039	14·34	18·44	96
1/1·25	—	—	—	—	0·998	1·060	15·51	19·54	96
1/2	—	—	—	—	1·175	1·245	45·76	48·23	108
1/2·75	1·040	1·066	25·69	41·60	1·137	1·206	36·54	41·60	108
1/3	0·952	0·972	17·47	24·03	1·121	1·195	34·22	39·85	108

coexistence points thus obtained have been collected in table 7. Note that, as we have not made a systematic study of the system size dependence of the phase transitions all our results apply to system sizes of $\sim 10^2$ particles. A graphic illustration of the resulting 'phase diagram' is shown in figure 6. For the sake of completeness we have included the data of Hoover and Ree [1] on hard spheres in this figure. In figure 6 four different phases can be distinguished, viz. isotropic fluid, nematic fluid, orientationally ordered crystal and orientationally disordered ('plastic') crystal. The latter phase is only observed for the more spherical ellipsoids ($1{\cdot}25 \geqslant x \geqslant 0{\cdot}8$). The rotator phase has a face-centred cubic structure. As the orientationally disordered solid phase is approached from the ordered solid, the orientational order parameter, $S = \langle P_2(\cos\theta)\rangle$, appears to go to zero continuously. Moreover, we find no evidence for discontinuous changes in the density

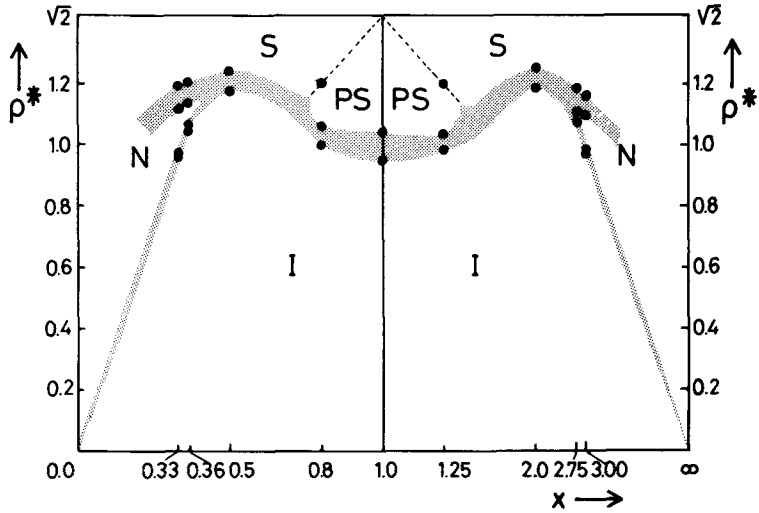

Figure 6. 'Phase diagram' of hard ellipsoids of revolution. Vertical axis: density in units $(8ab^2)^{-1}$, horizontal axis: length-to-breadth ratio, x. The shaded areas correspond to two-phase regions. The dots are the computed coexistence points (see table 7). The points for $x = 1$ were taken from [1]. The following phases can be distinguished: I, isotropic fluid; N, nematic fluid; S, orientationally ordered solid; PS, plastic solid.

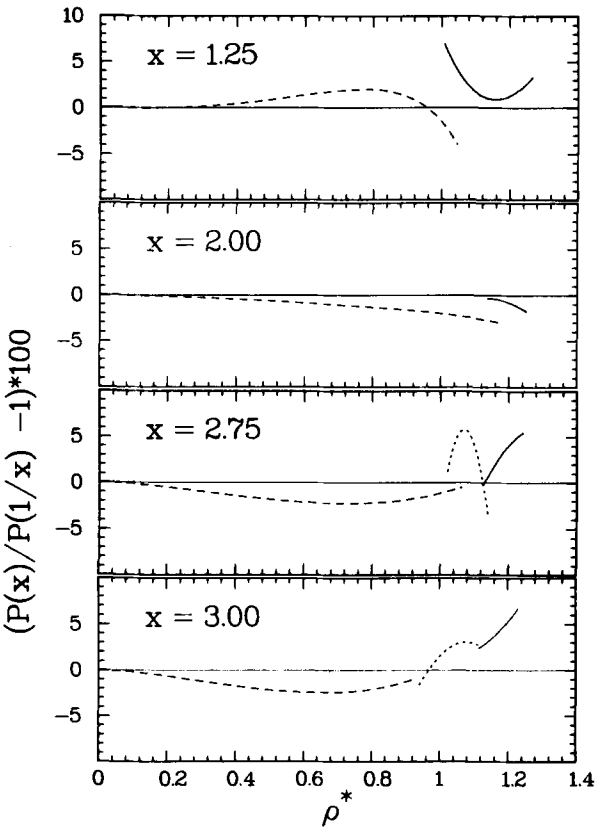

Figure 7. Deviation from perfect symmetry between the equations of state of hard ellipsoids of revolution with inverse length-to-breadth ratios. The vertical axis shows the percentual difference between the pressure of a fluid of HERs with $a/b = x$ at density ρ and the pressure for HERs with $a/b = x^{-1}$, at the same density. Dashed curve: isotropic branch; dotted curve: nematic branch; drawn curve: solid branch. The pressures used to draw these plots were obtained from the best fits to the Monte Carlo data (see table 6).

at the transition. We therefore identify the order-disorder transition in the solid as a higher order, or possibly weakly first order, phase transition. In figure 6 we have sketched the behaviour of the isotropic nematic transition in the limits $x \to 0$ and $x \to \infty$. As explained in the introduction, the I–N transition takes place at a packing fraction which goes to zero linearly with x or $1/x$ respectively. One of the more striking features of figure 6 is its high degree of apparent symmetry under interchange of x and $1/x$. This 'symmetry' is already present in the equation of state data. For all equation of state points studied, we find that the pressure at a given density for ellipsoids with a/b-ratio x and $1/x$ differs by at most 7 per cent. To visualize the symmetry in the equation of state data, we have plotted in figure 7 the density dependence of the percentual deviation of the pressure ratio $P(x)/P(1/x)$ from the value 1. At low densities this ratio approaches 1 because the second virial coefficients of HERs with length-to-breadth ratios x and $1/x$ are identical. However, at higher densities the ratio may differ from 1 because the third- and higher virial coefficients of HERs with $a/b = x$ and $a/b = 1/x$ have no

such symmetry [5, 8]. One should expect the asymmetry to become more pronounced as the ellipsoids become less spherical. It is however quite surprising to find that even for quite anisometric ellipsoids ($x = 3, 1/3$) the asymmetry is only a few per cent, even at densities where the virial series is expected to converge poorly, if at all. It should be added that symmetry in the phase diagram is not just to be expected at low densities but also at higher densities in those parts of the phase diagram where there is a high degree of orientational order (see [17]). In the subsequent paper [8] a comparison is made between the Monte Carlo data presented here and theoretical predictions based on the generalized y-expansion of Barboy and Gelbart [15].

We should like to thank Dr. J. P. McTague for his hospitality at the National Synchrotron Light Source in Brookhaven, where this work was started. One of us (B.M.M.) acknowledges financial support from 'Stichting FOM', which is funded by 'Nederlandse Organisatie voor Zuiver Wetenschappelijk Onderzoek (ZWO)'.

Appendix A

In this appendix we consider the free energy of our system in the presence of an external field, coupling to the orientation of the particles, to lowest order in the density. The free energy functional for this situation is given by

$$\beta F[\psi] = N\Big\{\int d\hat{\Omega}\psi(\hat{\Omega}) \ln \psi(\hat{\Omega}) + \ln \rho - 1 - \Lambda + \beta \int d\hat{\Omega}\psi(\hat{\Omega})u(\hat{\Omega}) + \sum_{n=2}^{\infty} \frac{B_n[\psi]}{(n-1)} \rho^{n-1}\Big\}. \quad \text{(A 1)}$$

Here $\psi(\Omega)$ is the one particle orientation distribution function with unit norm, $\hat{\Omega}$ a unit sector along the symmetry axis of the particles, ρ the number density, $u(\hat{\Omega})$ the external field and $B_n[\psi]$ a generalized virial coefficient. The equilibrium distribution is found by minimizing the free energy with respect to the function ψ, under the constraint that it be of unit norm. To lowest order in the density one simply finds

$$\psi_0(\hat{\Omega}) \sim \exp(-\beta u(\hat{\Omega})). \quad \text{(A 2)}$$

For our interaction we chose:

$$u(\hat{\Omega}) = -k \cos^2 \theta \equiv -k\xi^2, \qquad k > 0, \quad \text{(A 3)}$$

where θ is the angle between the molecular symmetry axis and the field direction. The next step is to calculate the second virial coefficient

$$B_2[\psi_0] = \frac{1}{2} \int d\hat{\Omega}\, d\hat{\Omega}' \psi_0(\hat{\Omega})\psi_0(\hat{\Omega})E(\hat{\Omega} \cdot \hat{\Omega}'). \quad \text{(A 4)}$$

Here $E(\hat{\Omega}' \cdot \hat{\Omega}')$ is the excluded volume of two ellipsoids with fixed orientations. This quantity can be developed in to a Legendre-polynomial series [18]

$$E(\hat{\Omega} \cdot \hat{\Omega}') = \sum_{l=0}^{\infty} \left(\frac{4l+1}{2}\right) e_l P_{2l}(\hat{\Omega} \cdot \hat{\Omega}'). \quad \text{(A 5)}$$

Explicit expressions for the coefficients e_l are found in the accompanying paper [8]. Turning to $\psi_0(\hat{\Omega})$ we will now consider its expansion. Defining $K = \beta k$ we have

$$\exp(K\xi^2) = \sum_{n=0}^{\infty} \frac{1}{n!} K^n \xi^{2n} = \sum_{n=0}^{\infty} \frac{1}{n!} K^n \sum_{l=0}^{n} \left(\frac{4l+1}{2}\right) c_{nl} P_{2l}(\xi), \tag{A 6}$$

where the coefficient c_{nl} are given by [19]

$$c_{nl} = \frac{n!\,\Gamma(n+\frac{1}{2})}{(n-l)!\,\Gamma(n+l+3/2)}, \tag{A 7}$$

$$\exp(K\xi^2) = \sum_{l=0}^{\infty} \left(\frac{4l+1}{2}\right) c_l P_{2l}(\xi), \tag{A 8}$$

with

$$c_l = \frac{\Gamma(l+\frac{1}{2})K^l}{\Gamma(2l+3/2)}\, {}_1F_1(l+\tfrac{1}{2},\, 2l+3/2,\, K). \tag{A 9}$$

Here a series representation for the confluent hypergeometric function was used [20]. Inserting these results into (A 4) one finds the desired correction to the free energy

$$B_2[\psi_0] = \frac{1}{2c_0^2} \sum_{l=0}^{\infty} \left(\frac{4l+1}{2}\right) e_l c_l^2. \tag{A 10}$$

References

[1] Hoover, W. G., and Ree, F. H., 1968, *J. chem. Phys.*, **49,** 3609.
[2] Frenkel, D., and Maguire, J. F., 1983, *Molec. Phys.*, **49,** 503.
[3] Onsager, L., 1949, *Ann. N.Y. Acad. Sci.*, **51,** 627.
[4] Kayser, R. F., and Raveché, H. J., 1978, *Phys. Rev.* A, **17,** 2067.
[5] Eppenga, R., and Frenkel, D., 1984, *Molec. Phys.*, **52,** 1303.
[6] Frenkel, D., Mulder, B. M., and McTague, J. P., 1984, *Phys. Rev. Lett.*, **52,** 287.
[7] Frenkel, D., Mulder, B. M., and McTague, J. P., 1985, *Molec. Crystals liq. Crystals*, **123,** 119.
[8] Mulder, B. M., and Frenkel, D., 1985, *Molec. Phys.*, **55,** 1193.
[9] Wood, W. W., 1968, *J. chem. Phys.*, **48,** 415.
[10] McDonald, I. R., 1972, *Molec. Phys.*, **23,** 41.
[11] Parrinello, M., and Rahman, A., 1980, *Phys. Rev. Lett.*, **45,** 1196.
[12] Several authors have independently developed similar Monte Carlo techniques. The first published account is: Najafabadi, R., and Yip, S., 1983, *Scripta metall.*, **17,** 1199.
[13] Vieillard-Baron, J., 1972, *J. chem. Phys.*, **56,** 4729.
[14] Perram, J. W., and Wertheim, M. S. (preprint). Perram, J. W., Wertheim, M. S., Lebowitz, J. L., and Williams, G. O., *Chem.* Phys. Lett., **105,** 277.
[15] Barboy, B., and Gelbart, W. M., 1979, *J. chem. Phys.*, **71,** 3053.
[16] Frenkel, D., and Ladd, A. J. C., 1984, *J. chem. Phys.*, **81,** 3188.
[17] Frenkel, D., 1985, *Molec. Phys.*, **54,** 145.
[18] Isihara, A., 1951, *J. chem. Phys.*, **19,** 1142.
[19] Gradshteyn, I. S., and Ryzhik, I. M., 1980, *Table of Integrals, Series and Products* (Academic Press), equation 8.2922 (1).
[20] [19], equation 9.210.